

# Novel Agglomeration Strategy for Elemental Sulfur Produced during Biological Gas Desulfurization

Annemerel R. Mol, Derek J. M. Meuwissen, Sebastian D. Pruijm, Chenyu Zhou, Vincent van Vught, Johannes B. M. Klok, Cees J. N. Buisman, and Renata D. van der Weijden\*



Cite This: *ACS Omega* 2021, 6, 27913–27923



Read Online

ACCESS |



Metrics & More

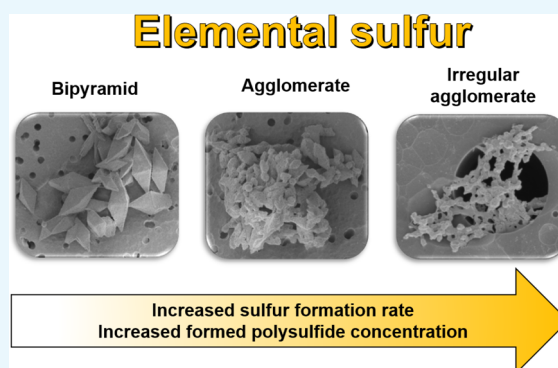


Article Recommendations



Supporting Information

**ABSTRACT:** This article presents a novel crystal agglomeration strategy for elemental sulfur (S) produced during biological desulfurization (BD). A key element is the nucleophilic dissolution of S by sulfide ( $\text{HS}^-$ ) to polysulfides ( $\text{S}_x^{2-}$ ), which was enhanced by a sulfide-rich, anoxic reactor. This study demonstrates that with enhanced  $\text{S}_x^{2-}$  formation, crystal agglomerates are formed with a uniform size ( $14.7 \pm 3.1 \mu\text{m}$ ). In contrast, with minimal  $\text{S}_x^{2-}$  formation, particle size fluctuates markedly ( $5.6 \pm 5.9 \mu\text{m}$ ) due to the presence of agglomerates and single crystals. Microscopic analysis showed that the uniformly sized agglomerates had an irregular structure, whereas the loose particles and agglomerates were more defined and bipyramidal. The irregular agglomerates are explained by dissolution of S by (poly)sulfides, which likely changed the crystal surface structure and disrupted crystal growth. Furthermore, S from  $\text{S}_x^{2-}$  appeared to form at least 5× faster than from  $\text{HS}^-$  based on the average  $\text{S}_x^{2-}$  chain length of  $x \approx 5$ , thereby stimulating particle agglomeration. In addition, microscopy suggested that S crystal growth proceeded via amorphous S globules. Our findings imply that the crystallization product is controlled by the balance between dissolution and formation of S. This new insight has a strong potential to prevent poor S settleability in BD.

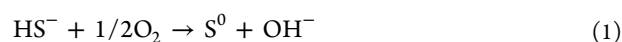


## 1. INTRODUCTION

Biomining, a process by which living organisms form a mineral, has a strong potential for resource recovery from waste streams. Elemental sulfur biomineralization specifically has been shown to be useful in removing hazardous hydrogen sulfide ( $\text{H}_2\text{S}$ ) from bio- and natural gas streams.<sup>1–3</sup> By transforming the toxic  $\text{H}_2\text{S}$  gas into elemental sulfur crystals, bacteria render the sulfide harmless and convert it into a valuable, safe, solid form that is easily recovered and reused. The sulfide-oxidizing bacteria (SOB) biomineralize elemental sulfur as an essential part of their energy metabolism using  $\text{H}_2\text{S}$  as electron donor. SOB naturally occur in a wide range of environments, such as hydrothermal vents, seas, sediments, lakes, and ponds,<sup>4–9</sup> yet in biological desulfurization (BD), they are present as biological catalysts. The elemental sulfur they produce, referred to as “biosulfur”, is especially useful as a fertilizer and fungicide, presumably because of its small particle size and hydrophilic properties.<sup>10–16</sup>

Based on the elemental sulfur biomineralization process, the Thiopaq BD technology was developed. Currently, more than 270 industrial installations have been built worldwide.<sup>17</sup> Typically, the process operates at mildly alkaline conditions (pH of 8.5) and elevated salinity (1 M). In the process, SOB oxidize the chemically absorbed  $\text{H}_2\text{S}$  to elemental sulfur by a

redox reaction with oxygen ( $\text{O}_2$ ) as the electron acceptor (eq 1)



In the bioreactor where the  $\text{O}_2$  is supplied via aeration, the  $\text{HS}^-$  can also be chemically oxidized to thiosulfate ( $\text{S}_2\text{O}_3^{2-}$ ) or biologically to sulfate ( $\text{SO}_4^{2-}$ ). However, these unwanted oxidation processes are largely prevented by carefully controlling  $\text{O}_2$  supply in the bioreactor with the redox potential so that elemental sulfur is the main product.<sup>1,18</sup>

While this BD process is an established biotechnology, the properties of the sulfur crystals formed are still hard to control. Analysis of several industrial BD installations has shown that the sulfur crystals vary greatly in particle size distribution (PSD) and morphology (aggregates, single crystals, or combinations thereof).<sup>19</sup> Sulfur aggregates were shown to have the best settleability, which is preferable for removal of the sulfur from the BD reactor. The lack of control over

Received: July 13, 2021

Accepted: September 28, 2021

Published: October 18, 2021



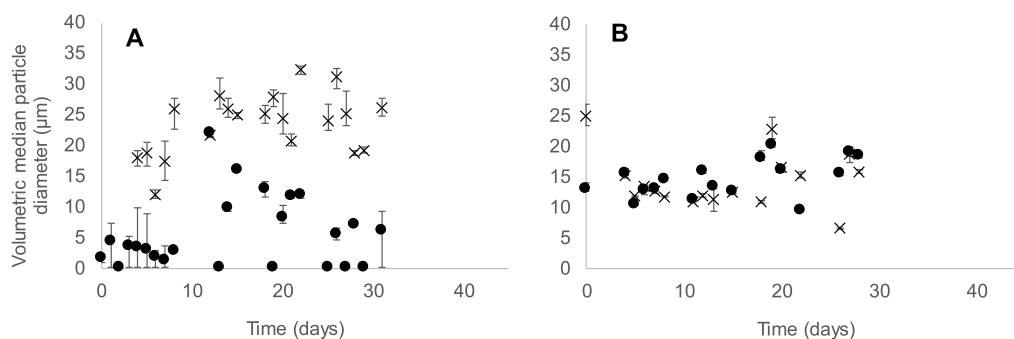


**Figure 1.** Development of median particle diameter from the gas-lift reactor (●) and from the settler (×) in exp. 1 (A, short polysulfide formation time) and 2 (B, long polysulfide formation time). The average median particle diameter for exp. 1 was  $5.6 \pm 5.9 \mu\text{m}$  from the gas-lift reactor and  $23.4 \pm 5.0 \mu\text{m}$  from the settler. The average median particle diameter for exp. 2 was  $14.7 \pm 3.1 \mu\text{m}$  from the gas-lift reactor and  $14.3 \pm 4.6 \mu\text{m}$  from the settler.

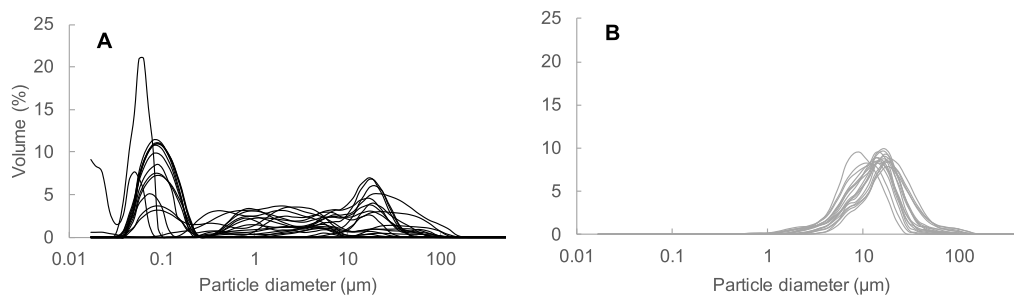
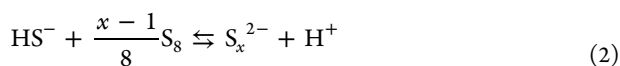


**Figure 2.** An overview of all PSDs from the gas-lift reactors shows a wide range of particle sizes for exp. 1 (A, short polysulfide formation time) in contrast with a narrow range of particle sizes for exp. 2 (B, long polysulfide formation time).

particle properties may hinder the sulfur settleability and subsequently may lead to operational problems, such as sulfur accumulation and foaming. The differences in particle size and morphology, which were qualified in previous work, could not be explained due to limited data available on the specific operating conditions under which the particles were formed such as the  $\text{H}_2\text{S}$  loading rate, redox potential, aging time, and pH. However, a study from the perspective of surface chemistry by Janssen et al. did point to the  $\text{H}_2\text{S}$  loading rate in the reactor as being of importance for the formation of sulfur aggregates.<sup>20</sup> Furthermore, recently, the traditional reactor configuration with a gas washer and aerated bioreactor was extended with a sulfide-rich, anoxic, stirred compartment as this was shown to enhance sulfur production and to avoid (thio)sulfate formation.<sup>21</sup> In this sulfidic, anoxic compartment, polysulfide formation takes place (eq 2)<sup>22–25</sup>



Polysulfides ( $\text{S}_x^{2-}$ ) are chains of zero-valent sulfur atoms with one sulfur atom of oxidation state  $-2$ . We hypothesize that the polysulfide formation has a distinct effect on the elemental sulfur crystallization. However, the effect of this additional process step on the sulfur crystallization has not been studied.

These findings on aggregation,<sup>20</sup> fluctuating products in the industry,<sup>19</sup> and recent new process design<sup>21</sup> warrant investigation in the sulfur biocrystallization processes and conditions that affect them. Long-term (16–40 days) laboratory bioreactor experiments at varying conditions and designs were performed, and the resulting biosulfur particles were characterized to clarify the biosulfur crystallization mechanism and its relationship with the applied conditions. This knowledge can be applied to control sulfur particle

properties, which is important for the sulfur recovery efficiency. Simultaneously, operational problems that now are faced in the industry will be prevented.

## 2. RESULTS

**2.1. Elemental Sulfur Particle Size Development by Laser Diffraction.** Two continuous bioreactor experiments with the same  $\text{H}_2\text{S}$  loading rate ( $138 \text{ mmol L}^{-1} \text{ day}^{-1}$ ) but with different reactor design were performed for 31 and 28 days (exps. 1 and 2). In exp. 1, the polysulfide formation time was only 5 min (the retention time in the absorber), whereas in exp. 2, the time was extended to 45 min by adding a sulfidic, anoxic reactor. During the polysulfide formation time, polysulfide was formed autocatalytically when elemental sulfur, sulfide, and polysulfide reacted together.<sup>26</sup> Hence, more polysulfide was formed in exp. 2. The (poly)sulfide-rich solution was continuously pumped to the gas-lift reactor where all (poly)sulfides were oxidized by the SOB predominantly to elemental sulfur. The size of the elemental sulfur particles from the gas-lift reactor and the bottom of the settler in both experiments was analyzed over time (Figure 1).

A striking difference in particle size appeared between the two experiments. In the gas-lift reactor with short polysulfide formation time (exp. 1), the particle size fluctuated, but on average, it stayed relatively small ( $5.6 \pm 5.9 \mu\text{m}$ ). In contrast, particles from the gas-lift reactor with long polysulfide formation time (exp. 2) had a stable size and were, on average, larger ( $14.7 \pm 3.1 \mu\text{m}$ ). The same pattern of the wide size distribution of exp. 1 and the narrow size distribution in exp. 2 was observed in the particles collected from the settler. In exp. 1, the particles from the settler were on average at least 4 times larger ( $23.4 \pm 5.0 \mu\text{m}$ ) than from the gas-lift reactor, whereas in exp. 2, they were in the same size range ( $14.3 \pm 4.6$

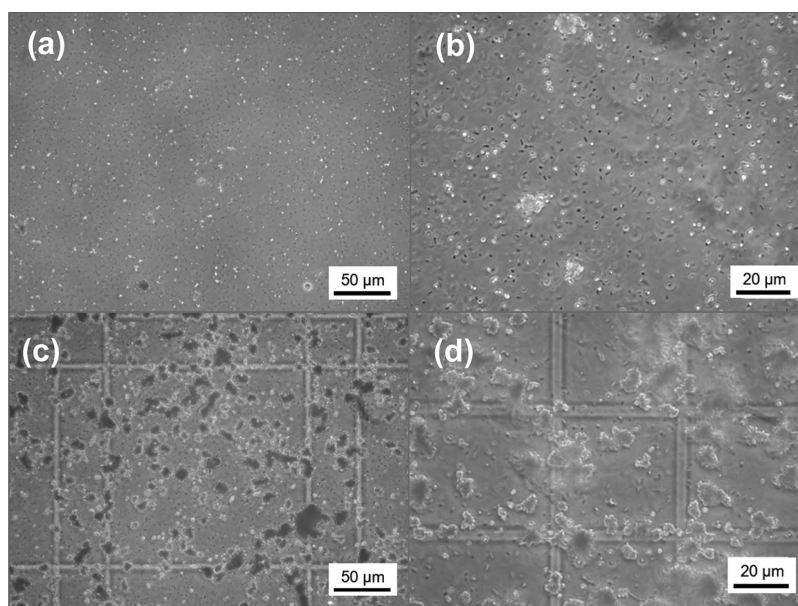


**Figure 3.** Light microscopy pictures of exp. 1 (short polysulfide formation time) (a) at day 19 and (b) at day 20 and of exp. 2 (long polysulfide formation time) (c) at day 19 and (d) at day 20. (a,c) 400 $\times$  magnification and (b,d) 1000 $\times$  magnification. The grid in c and d has no function in these pictures.

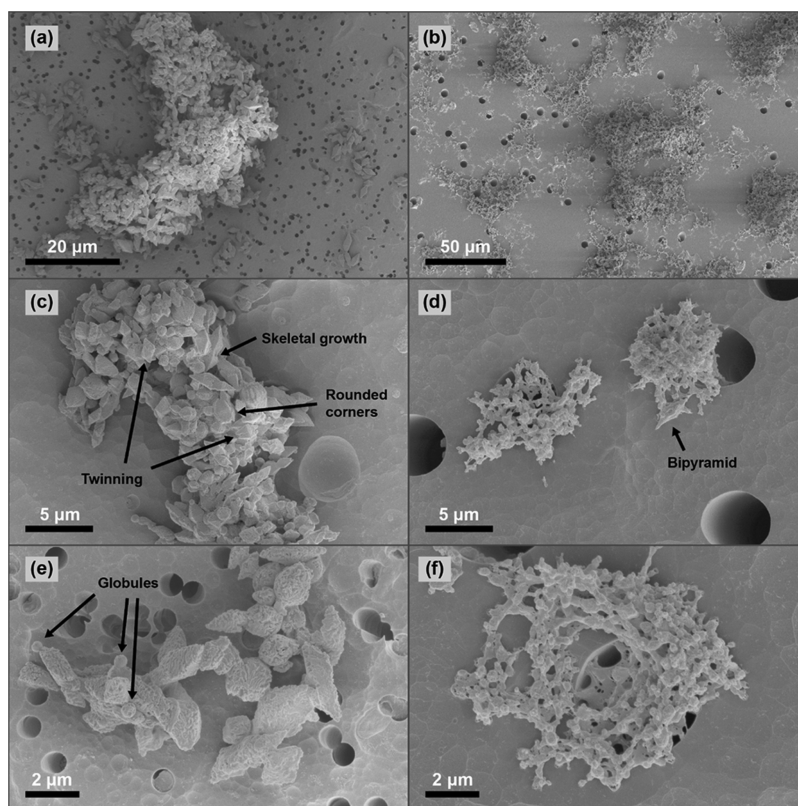


**Figure 4.** SEM pictures of elemental sulfur particles produced in exp. 1 with short polysulfide formation time (a,e: day 15, c: day 19) and exp. 2 with long polysulfide formation time (b,d,f: day 28) showing PSD (a,b), particle attachment (c,d), and crystal habit (e,f).

$\mu\text{m}$ ). This difference was also observed by light microscopy analysis (Supporting Information Figure S2). The wide (exp. 1) and narrow (exp. 2) full PSDs from the gas-lift reactor emphasized this strong difference between the size distribution of particles produced under the two different experimental conditions (Figure 2).

**2.2. Microscopic Analysis of Sulfur Particle Size and Morphology.** We first studied the morphology of the biosulfur particles from the gas-lift reactor with light microscopy and then selected two representative pictures for each experiment (Figure 3). Generally, biosulfur particles appeared as radiant, whitish shapes in the pictures. Thicker particles had darker, gray centers. Between the biosulfur



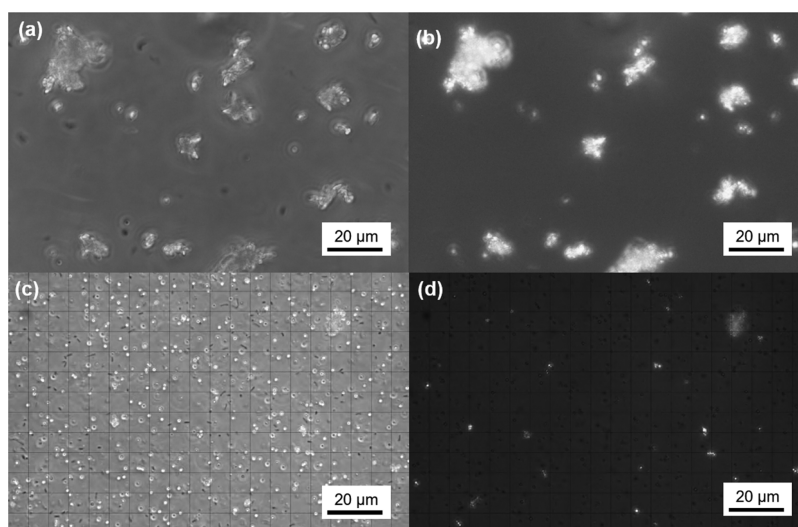


**Figure 5.** Polarized light microscopy revealed crystallinity of sulfur particles of exp. 1 due to the crystals' birefringence. (a,c) Without polarization filter. (b,d) With polarization filter. (a/b) Day 4 and (c/d) day 18. Sulfur globules of day 18 (c) are amorphous as they show no birefringence in (d). The grid in c and d has no function in these pictures.

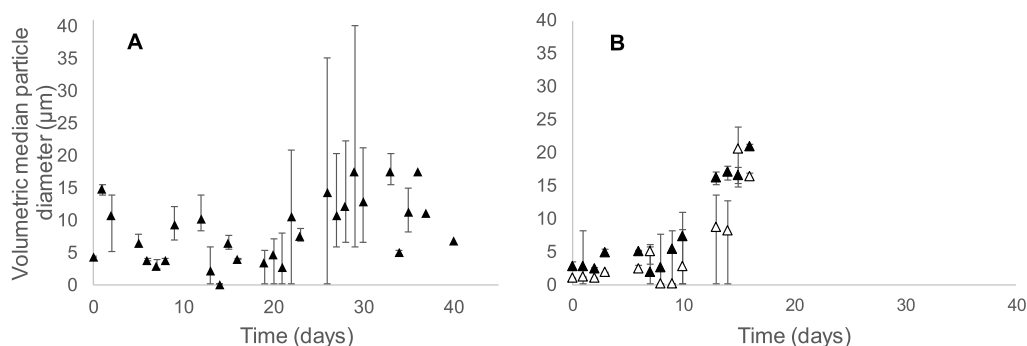


**Figure 6.** Development of the median particle diameter in expts. 3 (A) and 4 (B) (short and long polysulfide formation time without the settler). Particle diameters are shown for the gas-lift reactor (▲) and for exp. 4 also for the anoxic reactor (Δ). The average median particle diameter for exp. 3 was  $8.5 \pm 5.0 \mu\text{m}$ . The average median particle diameter for exp. 4 was  $8.2 \pm 6.9 \mu\text{m}$ . As clear growth was observed, the final median particle diameter for exp. 4 was  $20.9 \mu\text{m}$ .

particles, SOB from the mixed culture were identified as black dots (coccus), rods (bacillus), or spirals (spirochete). Sporadically, attachment of a globule-like sulfur particle to a microorganism was observed.

Although light microscopy did not provide the highest resolution, characteristic sulfur particle shapes were still identified. In exp. 1 (Figure 3a,b), most of the particles were single, although particle attachments were also present. The single particles were either roundish or bipyramidal. A bipyramidal crystal morphology is typical for orthorhombic  $\alpha$ -cyclo-octasulfur, which is most commonly found in nature.<sup>27</sup> The attachments were large ( $\sim 20 \mu\text{m}$ ) compared to the single particles ( $1\text{--}5 \mu\text{m}$ ). In contrast, in exp. 2 (Figure 3c,d), most of the particles seemed attached. Distinct crystal morphology was hardly visible; only at the edges of the attachments did we notice round particle profiles. The attachments were uniform in size ( $10\text{--}20 \mu\text{m}$ ) with an irregular, floc-like shape. The size distribution of the particles that was observed in the pictures corresponded well with the PSD as measured with laser diffraction. The pictures also showed that the larger particles in the PSD were particle attachments and that they were not single crystals.

For more detail on particle size and morphology, we analyzed the sulfur particles with scanning electron microscopy (SEM). Figure 5 illustrates the remarkable effect of polysulfide formation time on the PSD, particle attachments, and crystal habit. For the short polysulfide formation time (exp. 1), particles were either present as loose crystals or in attachments (Figure 4a). The single crystals were  $1\text{--}5 \mu\text{m}$ , and the attachments were  $5\text{--}60 \mu\text{m}$ . Especially, for the single crystals, the crystal habit was idiomorphically bipyramidal with a smooth surface, but imperfect bipyramids were also visible (Figure 4c). Examples of growth phenomena that we observed were rounded corners of the bipyramids, twinning, and skeletal growth (black arrows). This specific type of skeletal growth refers to the interconnected bipyramids as described by Desarnaud et al.<sup>28</sup> Other deviations from the idiomorphic bipyramidal shape were also observed, but we were not able to identify them. Moreover, globular particles were observed, which were attached to the crystal surface (black arrows, Figure 4e).

For the long polysulfide formation time (exp. 2), particles were predominantly present in porous, floc-like attachments of  $10\text{--}20 \mu\text{m}$  (Figure 4b). The crystal habit lacked bipyramidal shape (Figure 4d). Only one bipyramid (black arrow) was



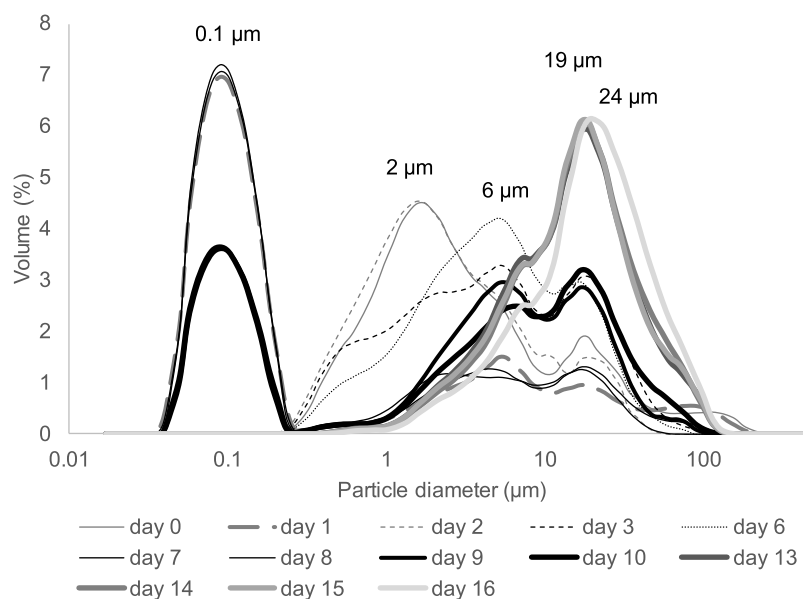


**Figure 7.** PSD development in exp. 4 (long polysulfide formation time, no settler). Peaks (modal particle diameters) are at 0.1, 2, 6, 19, and 24  $\mu\text{m}$ , showing gradual growth over the course of the experiment.

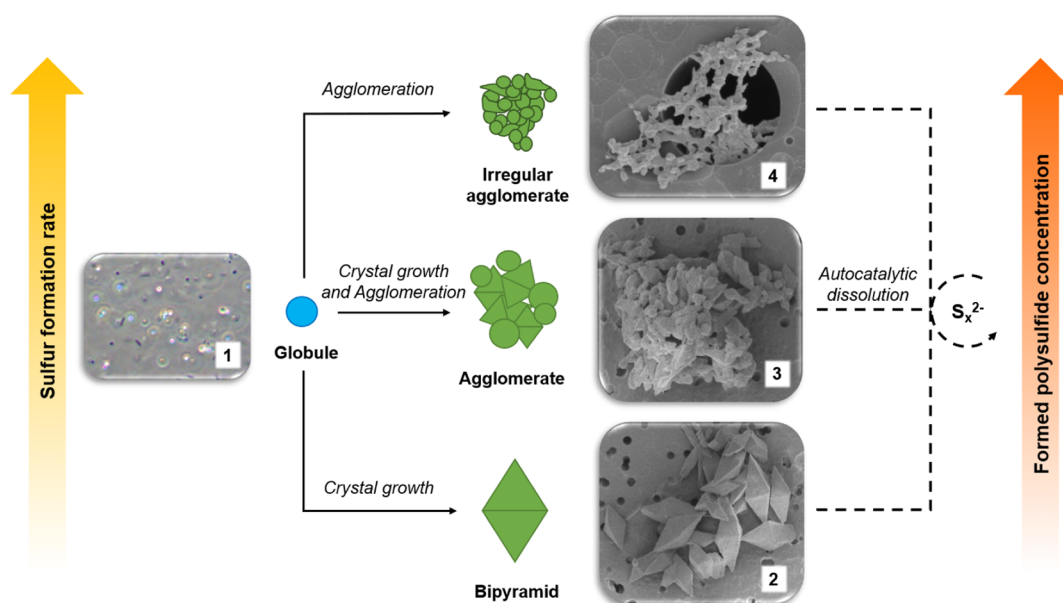


**Figure 8.** Proposed mechanism for elemental biosulfur crystal growth and agglomeration. First, an elemental sulfur globule is formed at the surface of an SOB and released into the solution (1). The globule may either grow to or become part of a bipyramidal crystal (2) at a low sulfur formation rate or agglomerate (3–4) at a moderate-to-high sulfur formation rate. At a moderate sulfur formation rate, the globules in the agglomerates may still crystallize and grow to the typical bipyramidal crystal shape (3), whereas at a high sulfur formation rate, this morphology is completely absent (4). In addition to growth, autocatalytic sulfur particle dissolution to (and by) polysulfides may take place that reduces the size of the sulfur particles and impedes formation of the bipyramidal crystal shape. The sulfur formation rate increases when more polysulfides are formed.

distinguished in Figure 4d, which seemed to be in the process of formation. Instead, the habit looked irregular and was characterized by round particles attached by bridge-like structures or cemented together (Figure 4f). Based on the pictures, the attachments from exp. 2 also appear to have a higher specific surface area than the particles and attachments from exp. 1. The round particles in the attachments of exp. 2 were much smaller in size (under 500 nm) than the particles in the attachments of exp. 1 (500 nm or larger).

Furthermore, the sulfur particles from exp. 1 were observed with polarized light microscopy (Figure 5). This technique

allows for the visual distinction between crystalline and amorphous materials due to a crystal's birefringence.<sup>29</sup> The sulfur crystals from day 4 (Figure 5a) are clearly visible under polarized light (Figure 5b), whereas the microorganisms in the sample are not visible because they are amorphous. On day 18, many globular particles were observed in the sample (Figure 5c). When those globules were inspected under polarized light, they were not visible (Figure 5d). This demonstrates that the globules are amorphous and not (yet) crystallized.

**2.3. Particle Size Development with a Lower  $\text{H}_2\text{S}$  Loading Rate and without a Settler.** The second set of

bioreactor experiments (experiment 3 and 4) did not need a settler by operating at a lower sulfide loading rate (i.e., 63 instead of 138 mmol L<sup>-1</sup> day<sup>-1</sup>). Exp. 3 was operated with a polysulfide formation time of 5 min, whereas for exp. 4, like exp. 2, the polysulfide formation time was extended to 39 min by adding an anoxic reactor. Despite the lower loading rate and the absence of the settler, in exp. 3 and 4, the same pattern as in exp. 1 and 2 was visible with respect to particle size (Figure 6). In exp. 3, the particle size shows large variations in the median diameter over time. In addition, variation between triplicate measurements was high, as shown by the large error bars. The average median particle size was  $8.5 \pm 5.0 \mu\text{m}$ , which was similar to exp. 1. In contrast, the sulfur particles from exp. 4 have a more uniform size. In exp. 4, the size of the particles from the anoxic reactor was also measured. Interestingly, the particle size was smaller than in the gas-lift reactor.

In addition, in exp. 4, we observed that the particle size increased over the course of the experiment (Figure 7). The median particle diameter grew, but the modal particle diameter also shifted from 0.1 to 24  $\mu\text{m}$  over time. The population of particles creating the peak at 0.1  $\mu\text{m}$  was mostly present at the beginning of the experiment and had disappeared by day 13. From day 13 onward, the PSD was like the PSDs in exp. 2.

### 3. DISCUSSION

In this study, we investigated the formation and growth of elemental sulfur crystals in biological gas desulfurization. In addition, we studied the effect of polysulfide formation time on biosulfur crystal growth. At long polysulfide formation time, uniformly sized particle attachments were formed, and their size was stable throughout the experiment. At short polysulfide formation time, particle attachments and single crystals were formed, resulting in a broad size range. At half the H<sub>2</sub>S dosing rate, the same particle size pattern was observed. However, in the experiment with half the H<sub>2</sub>S dosing rate and long polysulfide time (exp. 4), an increase in the particle size over time was observed. By day 13 of exp. 4, the PSD was similar to that of the experiment with a high H<sub>2</sub>S dosing rate and long polysulfide formation time (exp. 2). With respect to the particle morphology, the attachments at long polysulfide formation time were irregular (Figure 4b,d,f). In contrast, the attachments and particles at short polysulfide formation time were more organized and had a typical bipyramidal shape for orthorhombic  $\alpha$ -cyclo-octa sulfur (Figure 4a,c,e). Globular sulfur particles of varying size but all <1  $\mu\text{m}$  were also observed in the samples. When we analyzed the sulfur globules with polarized light microscopy, they showed no birefringence. This meant that the globules were amorphous, as opposed to the nonglobular particles in the sample, which were crystalline.

**3.1. Sulfur Crystal Growth Mechanism.** Based on these results, we propose an elemental biosulfur crystal growth mechanism in BD. The mechanism is derived from four types of sulfur particles observed during the experiments (Figure 8): globules, bipyramidal crystals, agglomerates, and irregular agglomerates of particles. The final size and shape of the sulfur particles depend not only on the sulfur formation rate but also on the dissolution of the elemental sulfur by polysulfide formation (indicated by upward arrows). Moreover, the crystal growth mechanism depends on the thermodynamic driving force, as upon entering the gas-lift reactor, the process solution is out of equilibrium and supersaturated. In electrochemical precipitation, this driving force is the potential of the actual concentration of ions in

solution compared to the equilibrium amount. As in our system we have both sulfide and polysulfides and we assume constant biological oxidation capacity of SOB, their electrochemical potential and concentrations will greatly determine the rates of sulfur solid formation when redox conditions change in the gas-lift reactor.<sup>30,31</sup>

The elemental sulfur globules (Figure 8-1) were observed throughout all experiments to be the initial phase of the sulfur crystallization. They were observed free in the solution, but sometimes, they were also observed attached to the SOB. Extracellular sulfur globule production by SOB has been previously reported.<sup>20,32–34</sup> Janssen et al. studied sulfide oxidization under similar conditions as those applied in our experiments. In their study, they documented SOB with sulfur globules on their surface in detail with cryo-SEM.<sup>20</sup> They also deduced that due to their negative surface charge, the sulfur particles must be covered with organic components. We did not study this, but the organic coating might affect the crystallization and stabilize the amorphous phase. Marnocha et al. also found that the globules of the SOB from their study are covered by a layer of organics (protein and polysaccharides), which is the main feature that distinguishes them from abiotically produced globules.<sup>34</sup> The organic coating on the globules appeared to slow the aging and crystallization of the amorphous sulfur globules. However, the globules in their study eventually transitioned to a more crystalline phase like the sulfur globules found in our experiments. Earlier research by the same group also indicated that globules could be formed without direct attachment to the SOB.<sup>33</sup> The globule formation in their study took place unattached from the cell by biologically produced polysulfides as an intermediate. However, Marnocha et al. studied a pure culture of one specific phototrophic SOB (*Chlorobaculum tepidum*) under purely anoxic conditions, whereas we studied sulfur formation by a mixed culture with a dominance of *Thioalkalivibrio* in the presence of oxygen. As the type of SOB and conditions differed, the globules may have formed in a different way. In our experiments, both attached and unattached formation may have occurred because we observed globule–SOB attachment and also many globules that were not attached to SOB. The most likely explanation is that the free globules in our experiments had been formed at the cell surface, but detached from the cell after formation. Nevertheless, the sulfur globules were the initial solid phase of elemental sulfur that was observed in our experiments. During and shortly after formation, the globules were still amorphous and may crystallize to elemental sulfur crystal nuclei. Therefore, from a crystallization point of view, they might be described as amorphous precursors.<sup>35</sup> We suggest that crystal growth proceeds via these globular amorphous precursors.

The second type of particles we found were idiomorphic bipyramidal crystals (Figure 8-2). A bipyramidal crystal morphology is typical for orthorhombic  $\alpha$ -cyclo-octasulfur. Not all bipyramids that were observed were idiomorphic; defects also occurred, such as rounded corners, twinning, (skeletal) hopper growth, and other unidentified defects (Figure 4c). With light microscopy and SEM, we frequently observed the attachment of a globule to a bipyramid. As elemental sulfur has an extremely low solubility of 19 nM at 25 °C,<sup>36</sup> it is not likely that crystal growth proceeded by the attachment of single aqueous S<sub>8</sub> rings. Instead, we suggest that crystal growth takes place by attachment of the globular amorphous precursors.<sup>37</sup> The reduction of surface energy is the

driver for this process. The idiomorphic shape of the bipyramids implied a slow growth process at low supersaturation in the metastable zone. As the globular amorphous precursors are suggested as the growth units, it is likely that the bipyramids were formed when the concentration of these globules was low. Moreover, the crystallization process for bipyramidal crystals should not be disturbed by, for example, nucleophilic attack of (poly)sulfide to the bipyramid as this would disturb the idiomorphic bipyramid shape. Formed polysulfide concentration was low due to a short retention time of the particles under anoxic, sulfidic conditions, for example, when only a gas absorber was present in the setup.

The third type of particles found in the experiments were sulfur crystal attachments (Figure 8-3). We had previously called these attachments to be aggregates,<sup>19</sup> but by definition of Lewis et al., they should be defined as agglomerates.<sup>38</sup> Unlike aggregates, agglomerates are built of individual crystals that are irreversibly cemented together. These agglomerates are thought to be formed by an accelerated crystallization process, where the globules do not have time to completely merge with the bipyramid to which they have adhered. By this process, the globules facilitate agglomeration through crystal bridging.<sup>39,40</sup> Defects in which a crystal grows attached to other crystals can also be described as a type of agglomeration.<sup>41</sup> Due to the extremely low solubility of elemental sulfur and the used H<sub>2</sub>S dosing rate (63–138 mmol L<sup>-1</sup> day<sup>-1</sup>), there was a constant tendency for high supersaturation. At high supersaturation and for relatively small crystals (e.g., with sizes up to 20 μm), agglomeration is frequently encountered in crystallization processes.<sup>42</sup> In addition, we postulate that polysulfide formation might alter the surface properties of the sulfur particles, thereby also stimulating agglomeration. Thus, the agglomeration process is expected to take place even at moderate sulfur formation rates.

The fourth type of particles we found were highly irregular agglomerates, which may also be defined as agglomerates (Figure 8-4). These agglomerates have lost any morphology that would indicate that they are elemental sulfur. The growth of these irregular agglomerates is thought to proceed by globule attachment in the gas-lift reactor, but is continuously disrupted by polysulfide formation. Being severely affected by this dissolution reaction to polysulfide, they hardly display typical sulfur morphology. Interestingly, these agglomerates had a stable size during the experiments. Moreover, the particle size in the anoxic reactor was structurally smaller than in the gas-lift reactor (exp. 4). The smaller size supports the argument that the agglomerates either were dissolved or reduced in size in the anoxic reactor due to polysulfide formation. In the gas-lift reactor, sulfur particles grew again as sulfur was formed by (poly)sulfide oxidation. The continuous cycle of breakdown and buildup of these particles led to the elimination of the small single particles and produced agglomerates of a stable size.

**3.2. Specific Role of Polysulfide Formation in Elemental Biosulfur Crystallization.** Our experiments show that polysulfides have a key role in the formation and growth of elemental sulfur. Kleinjan et al. and Hartler et al. both found that the presence of polysulfide ions accelerated the dissolution of elemental sulfur. Thereby, they affirmed that the formation of polysulfide ions has an autocatalytic effect on the rate of sulfur dissolution in aqueous sulfide solutions.<sup>26,43</sup> Therefore, supported by their findings, we suggest that the autocatalytic nucleophilic dissolution of elemental sulfur by

(poly)sulfides was likely to change the sulfur surface structure and disrupts the crystal growth process. This process may have formed (irregular) agglomerates. As the reaction is autocatalytic, longer polysulfide formation time and the continuous presence of polysulfide in the anoxic reactor will enhance the polysulfide formation. It is not clear how the polysulfide formation affected the surface structure exactly. However, in the SEM pictures, the surface of the particles which was exposed to long polysulfide formation time looked roughened. The roughness may have originated from uneven surface dissolution. Polysulfides may also have altered the particle surface by adsorption due to their bola-amphiphilic structure<sup>44,45</sup> or may have been attached to the surface as an effect of the polysulfide formation pathway.<sup>46</sup> In this pathway proposed by Kafantaris and Druschel, the nucleophilic dissolution of S<sub>8</sub> takes place either at the surface of the particle (surface reaction-controlled) or in the solution with solubilized S<sub>8</sub> rings (dissolution-controlled). In addition, the globules and/or crystals may be damaged or destabilized by polysulfide formation. This might enhance their agglomeration tendency as the hydrophilic layer of the particle is likely damaged by the nucleophilic attack of (poly)sulfides, stimulating hydrophobic sulfur–sulfur interactions.

Moreover, elemental sulfur formation from polysulfides is expected to have occurred substantially faster than from sulfide. The average chain size of polysulfide was previously reported to be  $5.17 \pm 0.03$  at an oxidation reduction potential (ORP) of  $-410$  mV under typical process conditions (pH of 8.5 and 35 °C).<sup>47</sup> Hence, the orthorhombic  $\alpha$ -S<sub>8</sub> formation rate from polysulfide is expected to go at least 5× faster than from HS<sup>-</sup> based on the approximate average polysulfide chain length of five. Elemental sulfur formation from polysulfides thus led to a higher sulfur formation rate, thereby stimulating agglomeration. In addition, Banciu et al. showed that SOB oxidize the sulfane atom (charge  $-2$ ) of S<sub>x</sub><sup>2-</sup> faster than HS<sup>-</sup> alone. When the final oxidation product of polysulfides is elemental sulfur, the formation of elemental sulfur is expected to go more than 5× faster from polysulfide than from HS<sup>-</sup>.<sup>48</sup> Furthermore, van den Bosch et al. showed that the SOB oxidation rate was not limited by higher S<sub>x</sub><sup>2-</sup> concentrations, whereas it was limited by a higher HS<sup>-</sup> concentration.<sup>49</sup> This may also have allowed for a higher sulfur formation rate. However, Dahl reported that, virtually, nothing is known about the oxidation of polysulfides and their transformation into sulfur precipitates.<sup>50</sup> Theoretically, the transformation of polysulfides to elemental sulfur could be purely a chemical process as they are in equilibrium with elemental sulfur.<sup>44</sup> Yet, no (poly)sulfide was detected in the bulk of the solution in the gas-lift reactor during the experiments. This indicates that the (poly)sulfide conversion was instantaneous and, thus, more likely the result of biological oxidation than of an equilibrium shift upon oxidation of HS<sup>-</sup>. Polysulfide formation thus played an essential role in the elemental sulfur crystal growth mechanism.

**3.3. Implications and Future Work.** Our findings explain the large PSD differences in BD installations and have important implications for controlling the elemental biosulfur crystallization in industrial BD. A key element is the nucleophilic dissolution of elemental sulfur by sulfide to polysulfides. Polysulfide formation can function as a novel agglomeration strategy, which has a strong potential to solve the problem for poor sulfur settleability in BD. In the traditional BD configuration, a large variety of particle sizes



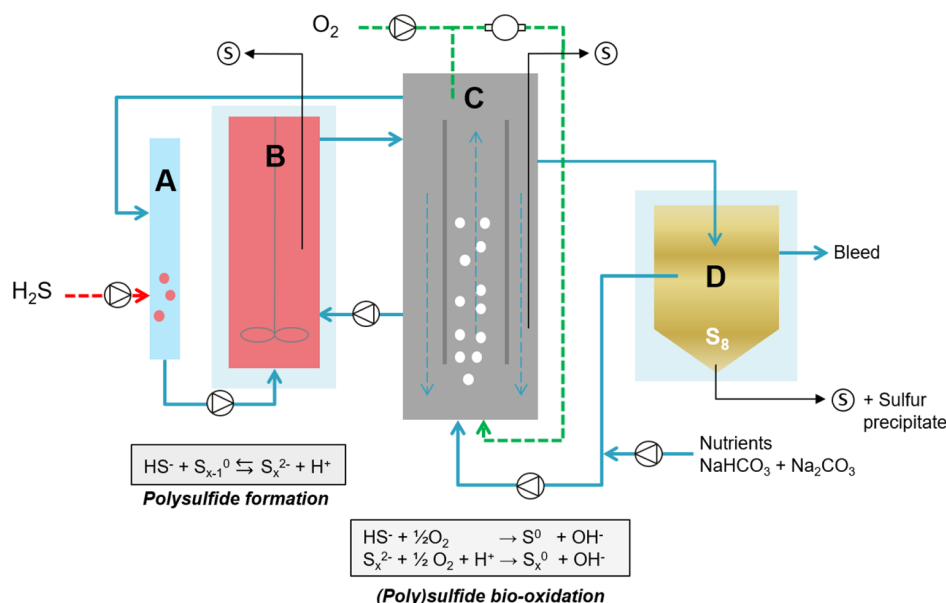


**Figure 9.** Experimental setup. (A) absorber, (B) anoxic reactor, (C) gas-lift reactor, (D) settler, and (S) sampling ports. For the design without compartment B, the liquid from the absorber A was introduced in the bottom of reactor C. Liquid flows are indicated with solid lines and gas flows with dashed lines. In compartments A and B, the main reaction taking place of interest to sulfur crystallization was polysulfide formation. In compartment C, the main reaction taking place of interest to sulfur crystallization was (poly)sulfide bio-oxidation.

and morphology was found with varying settleability.<sup>19</sup> Although larger crystal sizes could be reached by growing single crystals under low supersaturation, this is practically not feasible considering the high  $\text{H}_2\text{S}$  processing rates required in these types of processes. A more suitable approach would be to stimulate particle dissolution and agglomeration. Agglomerates as particles have better settleability than single crystals, but they also have less tendency to caking than single crystals.<sup>19,51</sup> Furthermore, agglomerates are filtered faster than single crystals.<sup>42</sup> Moreover, the apparent higher surface area of the agglomerates will be positive for the reactivity of elemental sulfur when it is applied as a fertilizer or fungicide. Despite these promising results, questions remain about which parameters control the exact size of the sulfur globules and when they are released from the SOB surface. We postulate that with a higher sulfur formation rate, the SOB produce smaller globules, which have a high tendency to detach from the SOB surface. In addition, the boundary operational conditions of the BD process needed to reach agglomeration are to be investigated. Besides, the field of nonclassical crystallization theory is still under development and the terminology therefore not well defined. This may lead to inaccurate use of terminology in our description. Future studies on these topics are therefore recommended.

#### 4. CONCLUSIONS

A novel agglomeration strategy has been developed for biologically produced elemental sulfur during biological gas desulfurization. Stable agglomeration was achieved by exposing formed elemental sulfur particles to sulfide in an anoxic environment in addition to the gas absorber so that the sulfur particles were partially dissolved to polysulfides. In the gas-lift reactor of the process, these (poly)sulfides were again oxidized to predominantly elemental sulfur. The agglomerates looked irregular and lacked a typical bipyramidal sulfur crystal shape. In contrast, when polysulfide formation time was short, the crystallization was less disturbed and a bipyramidal crystal

shape was observed. We thereby conclude that sulfur particle size and shape in the BD process depends on the degree of sulfur formation and dissolution to polysulfides. Furthermore, we postulate that the elemental sulfur crystallization proceeded via biologically formed amorphous sulfur globules. These findings may be used to control sulfur particle properties in industrial BD systems to enhance sulfur recovery and prevent operational issues.

#### 5. MATERIALS AND METHODS

**5.1. Experimental Setup.** Four reactor designs were used to produce elemental sulfur particles at two different  $\text{H}_2\text{S}$  loading rates (63 and 138  $\text{mmol L}^{-1} \text{day}^{-1}$ ). The simplest design consisted of a gas absorber (A) and a gas-lift reactor (C) (Figure 9). For the other three experiments, the design was extended with either a stirred anoxic reactor (B) between the absorber and gas-lift reactor and/or a settler (D) after the gas-lift reactor (emphasized in blue boxes). The  $\text{H}_2\text{S}$  gas was introduced into the reactor system through an anoxic absorber. During operation, the reactor content (i.e., buffered medium, SOB, sulfur particles, and dissolved sulfur species) was continuously circulated over the entire reactor system.  $\text{O}_2$  was introduced into the system in the gas-lift reactor. In the extended design with the anoxic reactor (ABC), the anoxic reactor prolonged the residence time of sulfur particles under anoxic conditions before they were circulated to the gas-lift reactor. In the extended design with the settler (ACD or ABCD), the settler prevented sulfur accumulation in the system during experiments with the high  $\text{H}_2\text{S}$  loading rate. Sulfur accumulation causes several operational issues, such as foaming and clogging.<sup>19</sup>

Pure  $\text{H}_2\text{S}$  gas and oxygen were supplied by mass flow controllers (Brooks, 5850E series, 0–100  $\text{mL min}^{-1}$ , Brooks Instrument LLC, Hatfield, USA) in the absorber and gas-lift reactor, respectively. The gas flow was recycled from the headspace to the bottom of the gas-lift reactor with a vacuum pump to prevent any release of  $\text{H}_2\text{S}$  gas and to reach low

oxygen concentrations. If pressure built up in the reactor, excess gas was discharged via a water lock saturated with zinc acetate to capture any potentially present  $\text{H}_2\text{S}$ . The overall working volume of the combined reactors was 4.2–9.1 L, depending on the specific design. The volume of the gas absorber was 0.2 L. The volume of the gas-lift reactor was always 3.7 L as this volume largely defines the sulfide oxidizing capacity. Small differences in reactor volumes between experiments are due to varying volumes in, for example, tubing. For optimal biological activity, the reactors were operated at 35 °C using a thermostat bath and climate-controlled cabinet.

**5.2. Medium Composition.** The medium consisted of a buffer with 6.6 g  $\text{L}^{-1}$   $\text{Na}_2\text{CO}_3$  and 69.3 g  $\text{L}^{-1}$   $\text{NaHCO}_3$  in demineralized water at pH 8.5. Fresh buffer was supplied as a constant flow to maintain enough alkalinity in the system. Furthermore, a nutrient stock was supplied for biological growth, containing (in grams per 1 L of demineralized water):  $\text{K}_2\text{HPO}_4$ , 0.1;  $\text{MgCl}_2 \cdot 6\text{H}_2\text{O}$ , 0.0203;  $\text{NaCl}$ , 0.6;  $\text{CH}_4\text{N}_2\text{O}$ , 0.06 and 2 mL  $\text{L}^{-1}$  trace element solution, as described by Pfenning and Lippert.<sup>52</sup> Additionally, the medium in the absorber and anoxic reactor contained dissolved  $\text{H}_2\text{S}$  gas, mainly as bisulfide ( $\text{HS}^-$ ). Various concentrations of sulfate and thiosulfate were present in the medium as they may be formed in the experiments by (biological) oxidation.

**5.3. Microbial Inoculum.** The reactors were inoculated with a mixed culture of SOB obtained from an industrial BD facility operating under halo-alkaline conditions at the industrial wastewater treatment site Industrierwater Eerbeek B.V. (Eerbeek, The Netherlands).<sup>53</sup> A well-characterized SOB often present in industrial BD facilities is *Thioalkalivibrio*,<sup>21,54–56</sup> which was also present in our inoculum (Supporting Information Figure S1). The reactors were either inoculated with washed microorganisms or, for practical reasons, with the complete reactor content of a previous experiment. The sulfur particles already present in the reactor could have functioned as seeds on the initial day of the experiments, but due to the high sulfur formation rate and continuous operation, we expect this to be negligible for the sulfur crystallization in most parts of the experiments. The microorganisms were washed to inoculate them without adding pre-existing elemental sulfur from the industrial BD facility. For washing, the reactor content was centrifuged at 4500 rpm for 20 min (Firlabo, Froilabo, Paris, France). A pellet was formed with two layers: a bottom layer of elemental sulfur and a layer with microorganisms on top. The pellet with microorganisms was carefully washed off and used as the inoculum.

**5.4. Experimental Operation.** The experiments carried out with the various reactor designs and  $\text{H}_2\text{S}$  loading rates are numbered exps. 1–4 (Table 1). The polysulfide formation is based on the sum of residence times of reactor content in the absorber and anoxic reactor. First, the reactor setup was filled with the medium and inoculum, after which  $\text{H}_2\text{S}$  supply was started. During each experiment, the  $\text{H}_2\text{S}$  loading rate was kept constant. To maximize sulfur production, the ORP was set at –360 mV versus Ag/AgCl, which is a representative set point for BD.<sup>3,19,21</sup> The ORP set point was controlled by a proportional–integral controller, which regulated the oxygen supply rate. In all experiments, the setup was operated in continuous mode without interruption. A bleed stream was collected by overflow from the gas-lift reactor or settler. General process performance was monitored by a variety of

**Table 1. Experimental Designs for Minimal (Exps. 1 and 3) and Enhanced (Exps. 2 and 4) Polysulfide Formation with Combinations of Reactor Compartments (A) Absorber, (B) Anoxic Reactor, (C) Gas-Lift Reactor, and (D) Settler**

| process condition  | exp. 1 | exp. 2 | exp. 3 | exp. 4 |
|--|--------|--------|--------|--------|
| line-up (reactor compartments used)  | ACD    | ABCD   | AC     | ABC    |
| total volume (L)   | 5.6    | 9.1    | 4.2    | 7.6    |
| volumetric S-loading rate (mmol $\text{L}^{-1}$ day $^{-1}$ ) <sup>a</sup> | 138    | 138    | 63     | 63     |
| duration (days)  | 31     | 28     | 40     | 16     |
| polysulfide formation time (min)   | 4.8    | 45.0   | 4.8    | 38.7   |

<sup>a</sup>Per liter gas-lift reactor.

parameters (Supporting Information Table S1). Reactors were equipped with sensors for temperature and ORP (triple junction, platinum rod, glass electrode equipped with an internal Ag/AgCl reference electrode, ProSense, Oosterhout, The Netherlands).

**5.5. Sampling and Analysis.** Each day, liquid samples with suspended elemental sulfur particles were taken at a sampling port in the middle of the anoxic reactor, the gas-lift reactor, and from the bottom of the settler. The sampling ports from the anoxic and gas-lift reactor were flushed 3 times prior to sampling to obtain a representative sample. Methods to measure sulfate and thiosulfate concentrations, alkalinity, conductivity, and pH have been previously described elsewhere.<sup>19</sup> The process selectivity for elemental sulfur was calculated by the mass balance based on the  $\text{H}_2\text{S}$  supply and measurement of dissolved sulfur products formed.<sup>21,57</sup> The microorganism concentration was measured as the amount of total nitrogen as in De Rink et al.<sup>21</sup> This method is based on the absorbance of nitrophenol at 345 nm and performed with the TNTplus 826 persulfate digestion method (Hach Company, Loveland, Colorado, United States). The presence of biologically produced sulfur did not affect the total nitrogen results.<sup>3</sup>

**5.6. Characterization of Elemental Sulfur Particles.** The sampled elemental sulfur particles were analyzed for various characteristics. Each day, sulfur PSD, particle morphology by light microscopy, and elemental sulfur concentration were measured according to Mol et al.<sup>19</sup> To verify the crystallinity of the sulfur particles, a polarizer was used on the light microscope. Due to the anisotropic, birefringent characteristic of crystalline sulfur, it is possible to distinguish it from isotropic, amorphous sulfur. The median ( $D_{50}$ ) of the PSD was reported to show the particle size development over time. The median was used because it is relatively unaffected by extreme measurements and skewed distributions.<sup>58</sup> Sulfur particles from exps. 1 and 2 were also analyzed with SEM. The SEM procedure was performed according to Mol et al.,<sup>19</sup> with the exception that the samples were placed on a membrane filter (PC Nuclepore Ø 13 mm, size 1 and 5  $\mu\text{m}$ , Whatman plc, Maidstone, UK) and dried at room temperature.

## ■ ASSOCIATED CONTENT

### Supporting Information

The Supporting Information is available free of charge at <https://pubs.acs.org/doi/10.1021/acsomega.1c03701>.

Relative abundance of microbial inoculum as measured with next-generation sequencing (NGS), NGS protocol, light microscopy pictures of samples from settler of exps.

1 and 2, and table with operational and process parameters of exps. 1–4 (PDF)

## AUTHOR INFORMATION

### Corresponding Author

**Renata D. van der Weijden** – Environmental Technology, Wageningen University & Research, 6700 AA Wageningen, The Netherlands; Wetsus, European Centre of Excellence for Sustainable Water Technology, 8900 CC Leeuwarden, The Netherlands; Email: [renata.vanderweijden@wur.nl](mailto:renata.vanderweijden@wur.nl)

### Authors

**Annemereel R. Mol** – Environmental Technology, Wageningen University & Research, 6700 AA Wageningen, The Netherlands; Paqell B.V., 3542 AD Utrecht, The Netherlands; [orcid.org/0000-0002-8778-8982](https://orcid.org/0000-0002-8778-8982)

**Derek J. M. Meuwissen** – Environmental Technology, Wageningen University & Research, 6700 AA Wageningen, The Netherlands

**Sebastian D. Pruijm** – Environmental Technology, Wageningen University & Research, 6700 AA Wageningen, The Netherlands

**Chenyu Zhou** – Environmental Technology, Wageningen University & Research, 6700 AA Wageningen, The Netherlands

**Vincent van Vught** – Environmental Technology, Wageningen University & Research, 6700 AA Wageningen, The Netherlands

**Johannes B. M. Klok** – Environmental Technology, Wageningen University & Research, 6700 AA Wageningen, The Netherlands; Paqell B.V., 3542 AD Utrecht, The Netherlands; Wetsus, European Centre of Excellence for Sustainable Water Technology, 8900 CC Leeuwarden, The Netherlands

**Cees J. N. Buisman** – Environmental Technology, Wageningen University & Research, 6700 AA Wageningen, The Netherlands; Wetsus, European Centre of Excellence for Sustainable Water Technology, 8900 CC Leeuwarden, The Netherlands

Complete contact information is available at: <https://pubs.acs.org/10.1021/acsomega.1c03701>

### Notes

The authors declare no competing financial interest.

## ACKNOWLEDGMENTS

We thank Marcel Giesbers for performing SEM analyses and the Wetsus Sulfur Theme and the ETE-MIB Sulfur Thesis Ring for fruitful discussions and feedback. This work was financially supported by Paqell B.V.

## REFERENCES

- (1) Janssen, A. J. H.; Meijer, S.; Bontsema, J.; Lettinga, G. Application of the Redox Potential for Controlling a Sulfideoxidizing Bioreactor. *Biotechnol. Bioeng.* **1998**, *60*, 147–155.
- (2) Buisman, C. J. N.; Geraats, B. G.; Ijspeert, P.; Lettinga, G. Optimization of Sulphur Production in a Biotechnological Sulphide-Removing Reactor. *Biotechnol. Bioeng.* **1990**, *35*, 50–56.
- (3) Van Den Bosch, P. L. F.; Van Beusekom, O. C.; Buisman, C. J. N.; Janssen, A. J. H. Sulfide Oxidation at Halo-Alkaline Conditions in a Fed-Batch Bioreactor. *Biotechnol. Bioeng.* **2007**, *97*, 1053–1063.
- (4) Sorokin, D. Y.; Kuenen, J. G.; Muyzer, G. The Microbial Sulfur Cycle at Extremely Haloalkaline Conditions of Soda Lakes. *Front. Microbiol.* **2011**, *2*, 44.
- (5) Jørgensen, B. B.; Fossing, H.; Wirsén, C. O.; Jannasch, H. W. Sulfide Oxidation in the Anoxic Black Sea Chemocline. *Deep-Sea Res., Part A* **1991**, *38*, S1083–S1103.
- (6) Canfield, D. E.; Raiswell, R. The Evolution of the Sulfur Cycle. *Am. J. Sci.* **1999**, *299*, 697–723.
- (7) Sorokin, D. Y.; Tourova, T. P.; Lysenko, A. M.; Muyzer, G. Diversity of Culturable Halophilic Sulfur-Oxidizing Bacteria in Hypersaline Habitats. *Microbiology* **2006**, *152*, 3013–3023.
- (8) Bush, T.; Diao, M.; Allen, R. J.; Sinnige, R.; Muyzer, G.; Huismans, J. Oxidic-Anoxic Regime Shifts Mediated by Feedbacks between Biogeochemical Processes and Microbial Community Dynamics. *Nat. Commun.* **2017**, *8*(). <https://doi.org/10.1038/s41467-017-00912-x>. DOI: 10.1038/s41467-017-00912-x
- (9) Meier, D. V.; Pjevac, P.; Bach, W.; Hourdez, S.; Girguis, P. R.; Vidoudez, C.; Amann, R.; Meyerdierks, A. Niche Partitioning of Diverse Sulfur-Oxidizing Bacteria at Hydrothermal Vents. *ISME J.* **2017**, *11*, 1545–1558.
- (10) Zhao, F. J.; McGrath, S. P.; Hawkesford, M. J. Sulphur Nutrition and the Sulphur Cycle. *Inst. Arab. Crop. Res. Rep.* **2001**, 36–39.
- (11) Aula, L.; Dhillon, J. S.; Omara, P.; Wehmeyer, G. B.; Freeman, K. W.; Raun, W. R. World Sulfur Use Efficiency for Cereal Crops. *Agron. J.* **2019**, *111*, 2485–2492.
- (12) Zessen, E. V.; Janssen, A. J. H.; Keizer, A. D.; Heine, B.; Peace, J.; Abry, R. Application of THIOPAQ™ Biosulphur in Agriculture. *Proceedings of the British Sulphur Events 2004 Sulphur Conference*, Oct. 24–27, 2004; Barcelona, Spain, 2004; pp 57–68.
- (13) Ernst, W. H. O. Agricultural Aspects of Sulfur. In *Environmental technologies to treat sulfur pollution*; Lens, P. N. L., Hulshoff Pol, L., Eds.; IWA Publishing: London, 2000; p 355.
- (14) Janssen, A. J. H.; Keizer, A. D.; Lettinga, G. Colloidal Properties of a Microbiologically Produced Sulphur Suspension in Comparison to a LaMer Sulphur Sol. *Colloids Surf., B* **1994**, *3*, 111–117.
- (15) Fertipaq Natural Solutions. Fertipaq. <https://en.fertipaq.com/> (accessed March 30, 2021).
- (16) Ceradis Crop Protection. CeraSulfur SC. <https://ceradis.com/products/crop-protection/cerasulfur-sc/> (accessed March 30, 2021).
- (17) O’Callaghan, P.; Adapa, L. M.; Buisman, C. Analysis of Adoption Rates for Needs Driven versus Value Driven Innovation Water Technologies. *Water Environ. Res.* **2019**, *91*, 144–156.
- (18) Van den Bosch, P. L. F. Biological Sulfide Oxidation by Natron-Alkaliphilic Bacteria Application in Gas Desulfurization. Ph.D. Thesis, Wageningen University, The Netherlands, 2008.
- (19) Mol, A.; Weijden, R. D.; Klok, J. B. M.; Buisman, C. J. N. Properties of Sulfur Particles Formed in Biodesulfurization of Biogas. *Minerals* **2020**, *10*, 433.
- (20) Janssen, A.; De Keizer, A.; Van Aelst, A.; Fokkink, R.; Yangling, H.; Lettinga, G. Surface Characteristics and Aggregation of Microbiologically Produced Sulphur Particles in Relation to the Process Conditions. *Colloids Surf., B* **1996**, *6*, 115–129.
- (21) De Rink, R.; Klok, J. B. M.; van Heeringen, G. J.; Sorokin, D. Y.; ter Heijne, A.; Zeijlmaker, R.; Mos, Y. M.; de Wilde, V.; Keesman, K. J.; Buisman, C. J. N. Increasing the Selectivity for Sulfur Formation in Biological Gas Desulfurization. *Environ. Sci. Technol.* **2019**, *53*, 4519–4527.
- (22) Boulègue, J. Équilibres Dans Le Système H<sub>2</sub>S-S<sub>8</sub> Colloïde-H<sub>2</sub>O. *Acad. Sci., Paris, C. R.* **1976**, *283*, 591–594.
- (23) Chen, K. Y.; Gupta, S. K. Formation of Polysulfides in Aqueous Solution. *Environ. Lett.* **1973**, *4*, 187–200.
- (24) Stuedel, R. Inorganic Polysulfides S n<sup>2-</sup> and Radical Anions S n<sup>-</sup>. *Elemental Sulfur and Sulfur-Rich Compounds II*; Springer-Verlag: Berlin, Heidelberg, 2003; pp 127–152.
- (25) Kamyshny, A.; Gun, J.; Rizkov, D. A. N.; Voitsekovski, T.; Lev, O. Equilibrium Distribution of Polysulfide Ions in Aqueous Solutions at Different Temperatures by Rapid Single Phase Derivatization. *Environ. Sci. Technol.* **2007**, *41*, 2395–2400.



- (26) Kleinjan, W. E.; de Keizer, A.; Janssen, A. J. H. Kinetics of the Reaction between Dissolved Sodium Sulfide and Biologically Produced Sulfur. *Ind. Eng. Chem. Res.* **2005**, *44*, 309–317.
- (27) Steudel, R.; Eckert, B. Solid Sulfur Allotropes. In *Elemental Sulfur and Sulfur-Rich Compounds I*; Steudel, R., Ed.; Springer-Verlag: Berlin, Heidelberg, New York, 2003; pp 1–80.
- (28) Desarnaud, J.; Derluy, H.; Carmeliet, J.; Bonn, D.; Shahidzadeh, N. Hopper Growth of Salt Crystals. *J. Phys. Chem. Lett.* **2018**, *9*, 2961–2966.
- (29) Oldenbourg, R. Polarized Light Microscopy: Principles and Practice. *Cold Spring Harb. Protoc.* **2013**, *11*, 1023–1036.
- (30) Milchev, A. Nucleation Phenomena in Electrochemical Systems: Thermodynamic Concepts. *ChemTexts* **2016**, *2*, 1–9.
- (31) Sehgal, R. M.; Cogan, J. G.; Ford, D. M.; Maroudas, D. Onset of the Crystalline Phase in Small Assemblies of Colloidal Particles. *Appl. Phys. Lett.* **2013**, *102*, 201905.
- (32) Hanson, T. E.; Bonsu, E.; Tuerk, A.; Marnocha, C. L.; Powell, D. H.; Chan, C. S. Chlorobaculum Tepidum Growth on Biogenic S(0) as the Sole Photosynthetic Electron Donor. *Environ. Microbiol.* **2016**, *18*, 2856–2867.
- (33) Marnocha, C. L.; Levy, A. T.; Powell, D. H.; Hanson, T. E.; Chan, C. S. Mechanisms of Extracellular S 0 Globule Production and Degradation in Chlorobaculum Tepidum via Dynamic Cell – Globule Interactions. *Microbiology* **2016**, *162*, 1125–1134.
- (34) Marnocha, C. L.; Sabanayagam, C. R.; Modla, S.; Powell, D. H.; Henri, P. A.; Steele, A. S.; Hanson, T. E.; Webb, S. M.; Chan, C. S. Insights into the Mineralogy and Surface Chemistry of Extracellular Biogenic S 0 Globules Produced by Chlorobaculum Tepidum. *Front. Microbiol.* **2019**, *10*, 271.
- (35) Mirabello, G.; Ianiro, A.; Bomans, P. H. H.; Yoda, T.; Arakaki, A.; Friedrich, H.; de With, G.; Sommerdijk, N. A. J. M. Crystallization by Particle Attachment Is a Colloidal Assembly Process. *Nat. Mater.* **2020**, *19*, 391–396.
- (36) Boulègue, J. Solubility of Elemental Sulfur in Water at 298 K. *Phosphorus Sulfur Relat. Elem.* **1978**, *5*, 127–128.
- (37) De Yoreo, J. J.; Gilbert, P. U.; Sommerdijk, N. A.; Penn, R. L.; Whitelam, S.; Joester, D.; Zhang, H.; Rimer, J. D.; Navrotsky, A.; Banfield, J. F.; Wallace, A. F.; Michel, F. M.; Meldrum, F. C.; Cölfen, H.; Dove, P. M. Crystallization by Particle Attachment in Synthetic, Biogenic, and Geologic Environments. *Science* (80-.). **2015**, *349* (). <https://doi.org/10.1126/science.aaa6760>. DOI: 10.1126/science.aaa6760
- (38) Lewis, A.; Seckler, M.; Kramer, H.; van Rosmalen, G. 6.3 The Agglomeration Process. *Industrial Crystallization Fundamental and Applications*; Cambridge University Press, 2015; pp 132–133.
- (39) Mersmann, A.; Braun, B. Agglomeration. In *Crystallization Technology Handbook*; Mersmann, A., Ed.; Marcel Dekker, Inc.: New York, NY, USA, 2001; p 237.
- (40) Linnikov, O. D. Mechanism of Aggregation and Intergrowth of Crystals during Bulk Crystallization from Solutions. *Cryst. Res. Technol.* **2008**, *43*, 1268–1277.
- (41) Jones, A. G. Crystal Agglomeration and Disruption. *Crystallization Process Systems*; Butterworth-Heinemann: Oxford, 2002; pp 155–189.
- (42) Lewis, A.; Seckler, M.; Kramer, H.; van Rosmalen, G. 2.7 Degree of Agglomeration. *Industrial Crystallization Fundamental and Applications*; Cambridge University Press: Cambridge, 2015; p 48.
- (43) Hartler, N.; Libert, J.; Teder, A. RATE OF SULFUR DISSOLUTION SODIUM SULFIDE IN AQUEOUS SODIUM SULFIDE. *Ind. Eng. Chem. Process Des. Dev.* **1967**, *6*, 398–406.
- (44) Steudel, R.; Holdt, G.; Visscher, P. T.; van Gernerden, H. Search for Polythionates in Cultures of Chromatium Vinosum after Sulfide Incubation. *Arch. Microbiol.* **1990**, *153*, 432–437.
- (45) Kharma, A.; Grman, M.; Misak, A.; Domínguez-Álvarez, E.; Nasim, M. J.; Ondrias, K.; Chovanec, M.; Jacob, C. Inorganic Polysulfides and Related Reactive Sulfur Selenium Species from the Perspective of Chemistry. *Molecules* **2019**, *24*(). <https://doi.org/10.3390/molecules24071359>. DOI: 10.3390/molecules24071359
- (46) Kafantaris, F.-C. A.; Druschel, G. K. Kinetics of the Nucleophilic Dissolution of Hydrophobic and Hydrophilic Elemental Sulfur Sols by Sulfide. *Geochim. Cosmochim. Acta* **2020**, *269*, 554–565.
- (47) Roman, P.; Bijmans, M. F. M.; Janssen, A. J. H. Quantification of Individual Polysulfides in Lab-Scale and Full-Scale Desulfurisation Bioreactors. *Environ. Chem.* **2014**, *11*, 702.
- (48) Banciu, H.; Sorokin, D. Y.; Kleerebezem, R.; Muyzer, G.; Galinski, E. A.; Kuenen, J. G. Growth Kinetics of Haloalkaliphilic, Sulfur-Oxidizing Bacterium Thioalkalivibrio Versutus Strain ALJ 15 in Continuous Culture. *Extremophiles* **2004**, *8*, 185–192.
- (49) van den Bosch, P. L. F.; de Graaff, M.; Fortuny-picornell, M.; van Leerdam, R. C.; Janssen, A. J. H. Inhibition of Microbiological Sulfide Oxidation by Methanethiol and Dimethyl Polysulfides at Natron-Alkaline Conditions. *Appl. Microbiol. Biotechnol.* **2009**, *83*, 579–587.
- (50) Dahl, C. A Biochemical View on the Biological Sulfur Cycle. In *Environmental Technologies to Treat Sulfur Pollution: Principles and Engineering*; Lens, P. N. L., Ed.; IWA Publishing, 2019; Chapter 3, pp 55–96.
- (51) Jin, S.; Chen, M.; Li, Z.; Wu, S.; Du, S.; Xu, S.; Rohani, S.; Gong, J. Design and Mechanism of the Formation of Spherical KCl Particles Using Cooling Crystallization without Additives. *Powder Technol.* **2018**, *329*, 455–462.
- (52) Pfennig, N.; Lippert, K. D. Über Das Vitamin B12-Bedurfnis Phototropher Schwefelbakterien. *Arch. Microbiol.* **1966**, *55*, 245–256.
- (53) Janssen, A. J. H.; Lens, P. N. L.; Stams, A. J. M.; Plugge, C. M.; Sorokin, D. Y.; Muyzer, G.; Dijkman, H.; Van Zessen, E.; Luimes, P.; Buisman, C. J. N. Application of Bacteria Involved in the Biological Sulfur Cycle for Paper Mill Effluent Purification. *Sci. Total Environ.* **2009**, *407*, 1333–1343.
- (54) Kiragosyan, K.; Klok, J. B. M.; Keesman, K. J.; Roman, P.; Janssen, A. J. H. Development and Validation of a Physiologically Based Kinetic Model for Starting up and Operation of the Biological Gas Desulfurization Process under Haloalkaline Conditions. *Water Res. X* **2019**, *4*, 100035.
- (55) Muyzer, G.; Sorokin, D. Y.; Mavromatis, K.; Lapidus, A.; Clum, A.; Ivanova, N.; Pati, A.; d’Haeseleer, P.; Woyke, T.; Kyrpides, N. C. Complete Genome Sequence of “Thioalkalivibrio Sulfidophilus” HL-EbGr7. *Stand. Genomic Sci.* **2011**, *4*, 23–35.
- (56) Sorokin, D. Y.; van den Bosch, P. L. F.; Abbas, B.; Janssen, A. J. H.; Muyzer, G. Microbiological Analysis of the Population of Extremely Haloalkaliphilic Sulfur-Oxidizing Bacteria Dominating in Lab-Scale Sulfide-Removing Bioreactors. *Appl. Microbiol. Biotechnol.* **2008**, *80*, 965–975.
- (57) Klok, J. B. M.; Van Den Bosch, P. L. F.; Buisman, C. J. N.; Stams, A. J. M.; Keesman, K. J.; Janssen, A. J. H. Pathways of Sulfide Oxidation by Haloalkaliphilic Bacteria in Limited-Oxygen Gas Lift Bioreactors. *Environ. Sci. Technol.* **2012**, *46*, 7581–7586.
- (58) Field, A. 1.7.2.2. The Median. *Discovering statistics using SPSS*; SAGE Publications Ltd.: London, 2009; pp 21–22.